Local and global epidemic outbreaks in populations moving in inhomogeneous environments

Arturo Buscarino,[1] Luigi Fortuna,[1] Mattia Frasca,[1,*] and Alessandro Rizzo[2,3]

[1]*Dipartimento di Ingegneria Elettrica Elettronica e Informatica, University of Catania, 95124 Catania, Italy*

[2]*Dipartimento di Ingegneria Elettrica e dell'Informazione, Politecnico di Bari, 70126 Bari, Italy*

[3]*Department of Mechanical and Aerospace Engineering, New York University Polytechnic School of Engineering, Brooklyn, New York 11201, USA*

(Received 2 April 2014; revised manuscript received 1 October 2014; published 21 October 2014)

We study disease spreading in a system of agents moving in a space where the force of infection is not homogeneous. Agents are random walkers that additionally execute long-distance jumps, and the plane in which they move is divided into two regions where the force of infection takes different values. We show the onset of a local epidemic threshold and a global one and explain them in terms of mean-field approximations. We also elucidate the critical role of the agent velocity, jump probability, and density parameters in achieving the conditions for local and global outbreaks. Finally, we show that the results are independent of the specific microscopic rules adopted for agent motion, since a similar behavior is also observed for the distribution of agent velocity based on a truncated power law, which is a model often used to fit real data on motion patterns of animals and humans.

DOI: 10.1103/PhysRevE.90.042813 PACS number(s): 89.75.−k, 05.65.+b

I. INTRODUCTION

Agent-based models are fundamental tools to study the spreading of epidemic diseases [1–6]. In these models, agents represent individuals which may contract the disease, and their motion accounts for time-varying interactions responsible for the contagion process. Several models have been developed, where either a detailed description of the single individual's features or global assumptions on aggregated subgroups have been proved to be effective for description of the relevant phenomena [7]. In the existing models, individual motion may either occur in a continuous space [8,9] or be constrained over the links of a transportation network [1–3,10,11]. In the latter case, referred to as metapopulation models, individuals are structured into subpopulations localized at the network nodes, among which they move according to given mobility patterns. Metapopulation models, with their capability to explicitly account for the heterogeneity of the population, the social interactions among individuals, the complex mobility patterns, and the behavioral response to the presence of the disease, have become fundamental for prediction of the diffusion scenarios of pandemic spreading and, consequently, for definition of containment interventions [3,12–17]. Recently, another mechanism to incorporate time-varying interactions among the agents of an epidemic process, thus overcoming the main limitation of static interactions of network-based approaches [18–23], has been proposed in [24], where infection only propagates through packet transmission, so that the whole epidemic process is driven by flows in the network.

One major finding in metapopulation models is that, besides a standard local epidemic threshold regulating the onset of outbreaks at the subpopulation level, the system also exhibits a global invasion threshold, that is, even if the epidemic starts to spread only over a subpopulation (i.e., a town), eventually it will spread to a macroscopic fraction of the population (i.e., a region, a nation, or worldwide) if the mobility rate of individuals is high enough [1]. The critical mobility rate depends on the topological fluctuations of the substrate network, whereby macroscopic outbreaks are favored by heterogeneity in link distribution.

Metapopulation models restrict the motion to selected locations modeled as the nodes of a graph. Instead, in this work, we consider a population consisting of agents that move in a continuous two-dimensional space and introduce heterogeneity in the parameters that regulate the epidemic spreading. In more detail, we assume that the force of infection depends on the spatial coordinates of the plane. We consider the space divided into two regions and let the force of infection assume a different value in each of them. We show that either local or global outbreaks may appear, depending on the model parameters. The onset of a global epidemic invasion threshold is usually found in metapopulation models, where the population is fragmented in localized structures connected by individual mobility. We show that a global epidemic invasion threshold may also be revealed in agent-based epidemic models with motion in a continuous space and identify as a key element for the onset of this threshold a large spatial heterogeneity of the force of infection.

Differently from metapopulation approaches, which describe individual flows among different cities, our model accounts for epidemic spreading within a region with homogeneous density such as a large metropolitan area. In the proposed interpretation of the model, our results lead to the conclusion that an inhomogeneous distribution of the epidemic spreading and its geographical confinement may also arise in areas with homogeneous density.

II. MODEL

We consider N moving agents distributed in a planar space $\Gamma = \{(y_1, y_2) \in \mathbb{R}^2 : 0 \leqslant y_1 \leqslant L, 0 \leqslant y_2 \leqslant L\}$, with periodic boundary conditions. Agents are represented as point particles, and their positions and velocities at time t are indicated as $\mathbf{y}_i(t) = (y_{i1}(t), y_{i2}(t)) \in \Gamma$ and $\mathbf{v}_i(t) \equiv (v_i(t)\cos\theta_i(t), v_i(t)\sin\theta_i(t))$, $i = 1, \ldots, N$. The velocity

*mfrasca@diees.unict.it

modulus of agents is constant in time and equal for all individuals, i.e., $v_i(t) = v, \forall i = 1, \ldots, N$, and $\forall t$. At time $t = 0$, the N particles are distributed in random positions in the plane. At each time step, agents stochastically change their heading $\theta_i(t)$. Thus, positions and headings of agents are updated according to the rule

$$\begin{aligned} y_{i1}(t + \Delta t) &= y_{i1}(t) + v \cos\theta_i(t)\Delta t, \\ y_{i2}(t + \Delta t) &= y_{i2}(t) + v \sin\theta_i(t)\Delta t, \\ \theta_i(t + \Delta t) &= \xi_i(t + \Delta t), \end{aligned} \tag{1}$$

where Δt is the simulation step, and ξ_i are N independent identically distributed (i.i.d.) random variables drawn from a uniform probability distribution in the interval $[-\pi, \pi]$. In addition, to account for the realistic phenomenon of travels with time scales shorter than those related to the disease dynamics, we introduce the possibility of agents performing long-distance jumps. This aspect is modeled by defining a parameter $p_j \in [0,1]$ that quantifies the probability of an agent's performing a jump to a random position in the plane. In summary, at each time step, each agent evolves either following Eqs. (1) with probability $1 - p_j$ or performing a jump with probability p_j. In the latter case, the agent position is updated to a random point in Γ.

The proposed motion model is used to provide a simplified version of the mobility patterns observed in animals and humans. It captures an essential feature, that is, the dominance of frequent short-motion steps combined with less frequent, wider-motion steps. More realistic motion rules [25–28] have also been applied in the studies executed in this paper, obtaining very similar results. In particular, velocity moduli $v_i(t)$ are i.i.d. realizations of a random variable v with a truncated power-law probability density function with exponent $\beta = 1.59$. Realizations $v_i(t)$ of the random variable v are constrained between $v_{\min} = 0.1/\Delta t$, to avoid the singularity of the probability density function close to 0, and $v_{\max} = c\sqrt{2}L/\Delta t$, to model an upper bound on the agent velocity. The parameter c is a constant that is varied to account for different motion patterns.

Epidemic spreading is modeled according to the SIR model, which partitions the N agents into three disjoint compartments: susceptible (S), infective (I), and recovered (R). We indicate as $N_S(t)$, $N_I(t)$, and $N_R(t)$, respectively, the number of agents in the three compartments at time t, with the total number of agents $N_S(t) + N_I(t) + N_R(t) = N$, which remains constant in time. A small fraction of agents is set to the infective state at $t = 0$ to provide the seed of the infection, while all the others start from the susceptible state.

The process through which the disease spreads can be summarized as follows. An interaction radius defines the network of contacts: at each time step t each agent interacts only with the agents located within a disk-shaped neighborhood of radius D [8]. Without loss of generality, we set $D = 1$ in the remainder of the paper. The probability of infection of agent i depends on its position in space $\mathbf{y}_i$ and on the number of infected individuals in its neighborhood N_r^i, through the per-contact force of infection $\lambda(\mathbf{y}_i)$. Notably, if agent i is in the S state at time t, and exactly one of its neighbors is in the I state, i.e., $N_r^i = 1$, then agent i will move into the I state with probability $\lambda(\mathbf{y}_i)$ and remain in the S state with probability $1 - \lambda(\mathbf{y}_i)$. On the other hand, if $N_r^i > 1$, then its probability of being infected is $1 - (1 - \lambda(\mathbf{y}_i))^{N_r^i}$. Moreover, each infected agent will permanently move into the R (recovered) state with probability μ. This sets the average duration time of the infection as $\tau = 1/\mu$. Figure 1 shows the modeling framework adopted in this paper, where the space is partitioned into two regions, each corresponding to a different force of infection. Notably, $\lambda(\mathbf{y}_i) = \lambda_c$ if $\mathbf{y}_i \in \Gamma_c$, where Γ_c is a square $\Gamma_c = \{(y_1, y_2) \in \mathbb{R}^2 : 0 \leqslant y_1 \leqslant L_c, 0 \leqslant y_2 \leqslant L_c\}$ with $L_c \leqslant L$, and $\lambda(\mathbf{y}_i) = \lambda_e$ if $\mathbf{y}_i \in \Gamma \backslash \Gamma_c$. Hence, we consider λ_c and λ_e as model parameters. As agents move on the plane, the force of infection associated with each agent takes one of the two values, λ_c or λ_e, depending on the agent position at time t. To execute our analysis, two further parameters are taken into account: the agent density on the planar space, that is, $\rho = N/L^2$; and the ratio of the areas in which the plane is partitioned, that is, $\gamma = L_c^2/L^2$.

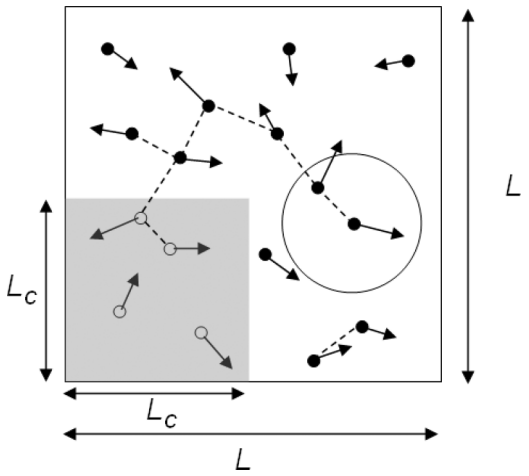

FIG. 1. Framework for the study of an epidemic in a population of agents moving into an inhomogeneous space. The D disk (representing the interaction area) is shown for only one agent. Dashed lines are drawn between neighboring agents.

III. RESULTS

To illustrate the system behavior, we first set the system parameters as $N = 10\,000$, $\rho = 3$, $v = 0.1$, $\mu = 0.15$, and $\gamma = 1/9$ and execute a set of simulations to study the steady-state fraction of recovered individuals R_∞ as a function of λ_c and λ_e, for three values of p_j (namely, $p_j = 0$, $p_j = 0.1$, and $p_j = 1$). In all the simulations in this paper we have set $\Delta t = 1$. Results are shown in Fig. 2. The major effect of the introduction of random jumps [Figs. 2(b) and 2(c)] on the steady-state fraction of recovered individuals is observed when a strong inhomogeneity exists between the two regions, that is, when λ_c and λ_e differ for several order of magnitudes. In particular, when the force of infection in Γ_c is much larger than in the rest of the plane, the presence of jumps imposes a great variability on R_∞. Notably, for $p_j = 0$ only a small fraction of the population contracts the disease, for $p_j = 0.1$ the fraction becomes more significant, and for $p_j = 1$ the epidemic spreads over almost all the individuals. Similarly, differences emerge

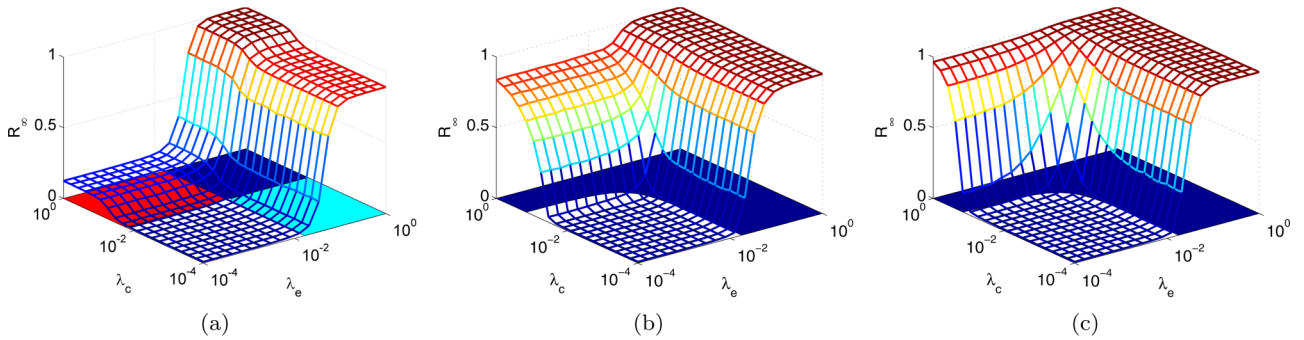

FIG. 2. (Color online) Steady-state fraction of recovered individuals R_∞ as a function of the parameters λ_c and λ_e. We have considered a system with $N = 10\,000$, $\rho = 3$, $D = 1$, $v = 0.1$, $\mu = 0.15$, $\gamma = 1/9$, and different values of p_j: (a) $p_j = 0$, (b) $p_j = 0.1$, and (c) $p_j = 1$. The floor represents theoretical expectations. In (a) the left (red) floor region corresponds to the occurrence of condition (5) in Γ_c; the right (cyan) region, in $\Gamma\backslash\Gamma_c$; and the top (dark-blue) region, in both Γ_c and $\Gamma\backslash\Gamma_c$. In (b) and (c) the dark floor area corresponds to condition (4) being satisfied (epidemic outbreak), while the white floor area corresponds to condition (4) not being satisfied (no epidemic outbreak). Simulations start with 1% of the agents set to the infective state. Results are averages over 50 runs.

when λ_c is very small, λ_e is large, and p_j is varied from 0 to 1. However, in this case variations are quite secondary, since the region characterized by a strong force of infection (that is, now $\Gamma\backslash\Gamma_c$) is larger than in the previous case (in fact, since $\gamma = 1/9$, Γ_c constitutes a small fraction of the entire plane).

To further elucidate the system behavior, we derive a mean-field approximation under the homogeneous mixing (HM) hypothesis, whereby each individual has the same probability of contacting any other. To this aim, we define $s(t) = N_S(t)/N$, $i(t) = N_I(t)/N$, and $r(t) = N_R(t)/N$ as the fractions of susceptible, infected, and recovered individuals at time t. Under the HM hypothesis, we calculate the probability of not being infected $\bar{p}_{\rm cont}$ and, then, the contagion probability as $p_{\rm cont} = 1 - \bar{p}_{\rm cont}$. The probability $\bar{p}_{\rm cont}$ that an agent is not infected by any of its neighbors is $\bar{p}_{\rm cont} = (1 - \lambda_c i(t))^a$ for agents located in Γ_c, while it is $\bar{p}_{\rm cont} = (1 - \lambda_e i(t))^a$ for agents located in $\Gamma\backslash\Gamma_c$, where $a = \pi D^2 \rho$ is the average number of neighbors. The fraction of susceptible individuals that enter the infected group at time $t + 1$ is $\gamma s(t)[1 - (1 - \lambda_c i(t))^a] + (1 - \gamma)s(t)[1 - (1 - \lambda_e i(t))^a]$. The first summand is the fraction of susceptible individuals in Γ_c [that is, $s(t)L_c^2/L^2$] multiplied by the contagion probability in that region. The second term is the fraction of susceptible individuals in $\Gamma\backslash\Gamma_c$ [that is, $s(t)(1 - L_c^2/L^2)$] multiplied by the contagion probability in that region. Thus, the fraction $i(t + 1)$ of infected individuals at time $t + 1$ is computed by considering that it is decreased by $\mu i(t)$ and increased by the fraction of susceptible individuals that become infected. The fraction of recovered individuals $r(t + 1)$ is obtained by considering that the increase in recovered individuals at time $t + 1$ is proportional to the number of infected individuals that recover, i.e., to $\mu i(t)$, while the fraction of susceptible individuals $s(t + 1)$ is computed from the conservation of the number of agents. Therefore, the complete mean-field model is

$$\begin{aligned} i(t+1) &= i(t) + \gamma s(t)[1 - (1 - \lambda_c i(t))^a] \\ &\quad + (1-\gamma)s(t)[1 - (1 - \lambda_e i(t))^a] - \mu i(t), \\ r(t+1) &= r(t) + \mu i(t), \\ s(t+1) &= 1 - i(t+1) - r(t+1), \end{aligned} \tag{2}$$

with $\gamma = L_c^2/L^2$.

We observe that the mean-field model, (2), is derived from basic principles of contact dynamics in epidemic processes. An alternate approach to the definition of a mean-field model can be grounded on the microscopic description of the agent dynamics, following the so-called individual-based modeling approach [29]. In this framework, blinking networks [30–33] can be a valuable modeling tool to describe the contact network. In the limit of high mobility ($p_j \to 1$ or, according to the terminology of blinking network, in the fast-switching hypothesis) the contact network is annealed into an averaged one that has its links weighted according to their activation probability, given in our case by $p = \pi D^2/L^2$ [34]. However, the relationship between deterministic models and descriptions at the individual level is far from being trivial, as discussed in [29].

From Eqs. (2), if the fraction of infected individuals at $t = 0$ is small, we can approximate $i(1)$ as

$$\begin{aligned} i(1) &= i(0) + \gamma s(0)\pi D^2 \rho \lambda_c i(0) + (1-\gamma)s(0)\lambda_e i(0) \\ &\quad - \mu i(0) + \mathcal{O}(i(0)) \end{aligned} \tag{3}$$

The condition for epidemic spreading is that the density of infected individuals increases over time, that is, $i(1) > i(0)$. Thus, an epidemic outbreak occurs if

$$\frac{\gamma\lambda_c + (1-\gamma)\lambda_e}{\mu} > \frac{1}{\pi D^2 \rho}. \tag{4}$$

We observe from Eq. (4) that the occurrence of an epidemic outbreak is favored by an increase in the density or in the interaction radius, since both factors contribute to the increase in the average node degree in the contact network, $\langle k \rangle = \pi D^2 \rho$. The parameter λ_c is weighted by γ, which is the ratio between the area of Γ_c and that of the total space [analogously, λ_e is weighted by $(1 - \gamma)$, which is the ratio between the area of $\Gamma\backslash\Gamma_c$ and that of Γ]. This implies that increasing the force of infection in only one of the two regions may not result in a global disease outbreak.

We expect that the HM hypothesis holds when the time scale of motion, dictated by p_j and v, is much shorter than that of the epidemic spreading process. In fact, when $p_j = 1$ the threshold condition [Eq. (4)] of the HM-based model accurately captures the system behavior. This can be

observed in Fig. 2(c), where the floor, representing theoretical expectations from the HM model, is in agreement with the numerical results. More precisely, the dark floor area indicates that condition (4) is satisfied, and, in correspondence to this, a macroscopic outbreak occurs. Thus, Eq. (4) clearly represents a global invasion threshold, that is, according to the definition in [1], a threshold for the onset of an epidemic involving the entire population.

Setting $p_j = 0$ drives the system far from the HM hypothesis. The large difference between λ_c and λ_e and the low mobility have the effect of splitting the populations into two parts, one confined in Γ_c and the other in $\Gamma\backslash\Gamma_c$, with distinct behaviors and a low level of mixing between them. Under these conditions the system behavior is governed by local epidemic thresholds, and as a consequence, the epidemic has different effects on the two subpopulations: the former undergoes an outbreak that involves the whole subpopulation (in Γ_c the size of the population is γN), and the latter is almost unaffected by the disease. To explain this behavior, we consider the limit case of zero mobility ($v \to 0$ and $p_j = 0$), whereby the agents remain confined either in Γ_c or in $\Gamma\backslash\Gamma_c$, and study the system behavior in each of the two regions, separately. Under these assumptions, each region is characterized by a contact network that is a random geometric graph with average node degree $\langle k\rangle = \pi D^2\rho$ and has a unique giant component for $\langle k\rangle \geqslant \ln(N_h)$, with $h = \{c,e\}$, and where $N_c = \gamma N$ and $N_e = (1-\gamma)N$ are the subpopulation sizes in Γ_c and $\Gamma\backslash\Gamma_c$, respectively [35]. The condition for an outbreak involving the whole subpopulation in any of the two zones is that a giant component appears and that

$$\frac{\lambda_h}{\mu} > \frac{1}{\pi D^2 \rho}, \tag{5}$$

where Eq. (5) is derived taking into account the expression for the epidemic threshold in a random network with $\langle k\rangle = \pi D^2\rho$ [36]. When Eq. (5) holds in Γ_c, the epidemic will involve a fraction of the population equal to γ, that is, $R_\infty = \gamma$, whereas, when Eq. (5) holds in $\Gamma\backslash\Gamma_c$, a steady-state fraction of recovered individuals $R_\infty = (1-\gamma)$ will be achieved. The theoretical prediction expressed in Eq. (5) is validated in Fig. 2(a). The floor colors indicate the occurrence of condition (5) in Γ_c [left (red) floor square], in $\Gamma\backslash\Gamma_c$ [right (cyan) floor square], or in both areas [top (dark-blue) floor square]. Even though condition (5) is derived under the hypothesis that agents are confined in Γ_c or in $\Gamma\backslash\Gamma_c$ in the absence of mobility, we find that the theoretical predictions also hold in the case of low mobility [$v = 0.1$ in Fig. 2(a). This is further illustrated in Fig. 3, where the system is simulated for a large value of λ_c ($\lambda_c = 1$) and a small value of λ_e ($\lambda_e = 10^{-2}$), that is, in a region of the parameter space which corresponds to the left (red) floor square in Fig. 2(a). Figure 3 illustrates simulation results for two density values: $\rho = 3$, which is greater than the threshold required to obtain a giant component in Γ_c, that is, $\rho > \ln(\gamma N)/\pi D^2 = 2.23$, and $\rho = 0.3$, which is below the threshold. The system clearly exhibits a global invasion threshold: when p_j is increased from 0 to 1, a transition between a regime characterized by local outbreaks and one characterized by a global invasion occurs. For $p_j = 0$ we observe the absence of outbreaks for $\rho = 0.3$ and an outbreak involving only a fraction of the population

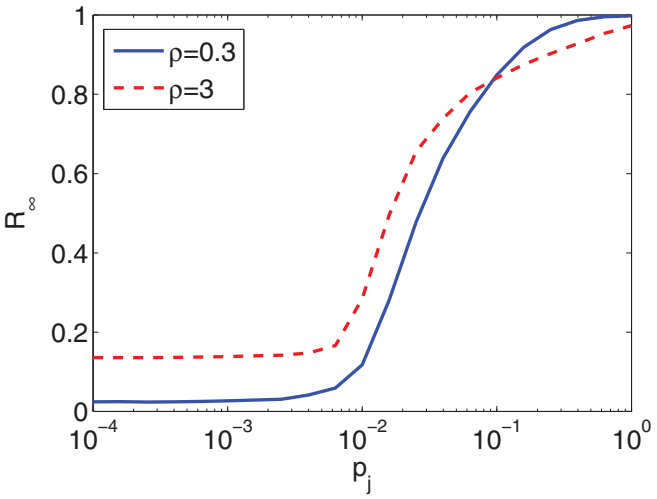

FIG. 3. (Color online) Steady-state fraction of recovered individuals R_∞ as a function of p_j for a system of $N = 10\,000$ agents with $\lambda_c = 1$ and $\lambda_e = 10^{-2}$, $\rho = 3$ [solid (blue) line] and $\rho = 0.3$ [dashed (red) line], $D = 1$, $v = 0.1$, $\mu = 0.05\rho$, and $\gamma = 1/9$. The system is started with a random 1% of the agents set in the infective state. Results are averages over 50 runs.

approximately equal to $R_\infty \simeq \gamma$ for $\rho = 3$, which indicates that the epidemic is almost confined in Γ_c and does not spread through the rest of the plane. When p_j is increased, the system transitions towards a regime over the global invasion threshold, and for both densities, the epidemic outbreak involves the entire population.

We further show the presence of two distinct regimes, obtained by varying the modulus v of the agent velocity according to a purely random walker model (that is, letting $p_j = 0$). Numerical results are illustrated in Fig. 4, which highlights the role of v in driving the system from a non-HM condition, obtained for a low velocity, to an HM condition, obtained for a high one. We observe that the role of v is analogous to that of p_j, yet they act on the system in different ways. In fact, increasing v implies a higher mobility for all the agents, whereas increasing p_j involves a higher fraction of agents that are likely to perform long-distance motion steps. The latter mechanism seems more effective in driving the system towards a HM condition, since it suffices that a few individuals gain the ability to jump, whereas a very high value of v for all agents is required when the purely random walker model is used. For low v, that is, in the case where the characteristic time of motion is no longer smaller than that of the epidemic process and mixing is not homogeneous, the behavior is ruled by the condition in Eq. (5). We also observe that, when mixing is not homogeneous, the number of contacts decreases and the epidemic threshold increases. Therefore, the threshold condition valid under the HM hypothesis [Eq. (4)] represents a lower bound for the epidemic spreading under nonfast motion.

We execute a further set of simulations to ascertain that the system behavior is not dependent on specific features of the motion model. Figure 5 shows the fraction of recovered individuals R_∞ as a function of λ_c and λ_e for the motion rule based on a truncated power-law distribution of agent velocities.

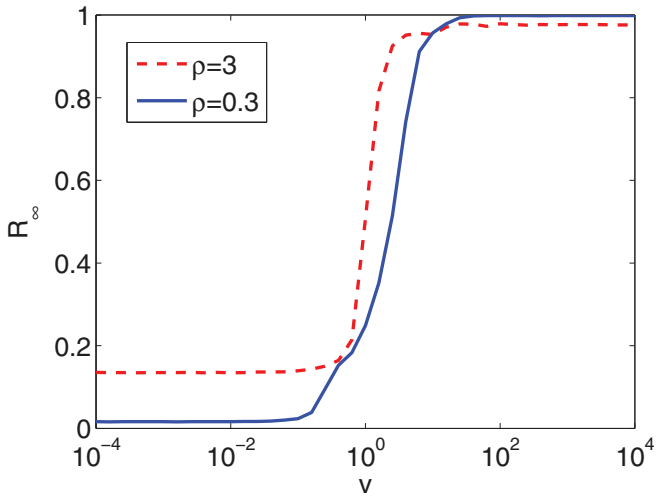

FIG. 4. (Color online) Steady-state fraction of recovered individuals R_∞ as a function of v for a system of $N = 10\,000$ agents with $\lambda_c = 1$ and $\lambda_e = 10^{-2}$, $\rho = 3$ [solid (blue) line] and $\rho = 0.3$ [dashed (red) line], $D = 1$, $p_j = 0$, $\mu = 0.05\rho$, and $\gamma = 1/9$. The system is started with a random 1% of the agents set in the infective state. Results are averages over 50 runs.

To account for different mixing levels we let the parameter c in the expression of the maximum velocity $v_{\max} = c\sqrt{2}L/\Delta t$ assume the values $c = 0.01$ [Fig. 5(a)], $c = 0.1$ [Fig. 5(b)], and $c = 1$ [Fig. 5(c)]. Numerical results illustrated in Fig. 5 are qualitatively similar to those in Fig. 2, since, for low mixing [Fig. 5(a)], outbreaks involve only one of the two regions Γ_c or $\Gamma\backslash\Gamma_c$. On the other hand, under homogeneous mixing [Fig. 5(c)], a global outbreak occurs when Eq. (4) holds. For intermediate values of the parameter c [Fig. 5(b)], the outbreak for small λ_e and large λ_c involves a significant percentage of the population but is not global. The major difference between the two motion rules comes from the comparison of Figs. 2(c) and 5(c), which shows that the transition to a global outbreak regime for low values of λ_e is sharper for the motion rule based on the combination of random walk and long-distance jumps. In fact, this model, although not capturing all the features of realistic motion patterns, allows us to study the system behavior under the ideal mixing hypothesis.

We now study the effect of targeted immunization strategies. Differently from most of the work presented in the literature, where a subset of individuals is selected to be immunized [36], here we study the effect of immunizing all the individuals that are located in a limited portion of the space. More specifically, we study the effect of a reduction of the force of infection λ_c in Γ_c. In this case, the effectiveness of the immunization strategy depends on the force of infection in the uncontrolled region (that is, on λ_e) and on the agent mobility: (i) for high λ_e and high mobility [Figs. 2(c) and 5(c)], decreasing λ_c has no effect on R_∞; (ii) for high λ_e and low mobility [Figs. 2(a) and 5(a)], reducing λ_c yields a reduction in the percentage of R_∞ only by an amount equal to the targeted fraction of the population, γ; (iii) for low λ_e and high mobility [Figs. 2(c) and 5(c)], reducing λ_c yields a total recovery of the population; and (iv) for low λ_e and low mobility [Figs. 2(a) and 5(a)], reducing λ_c controls the local outbreak, that is, R_∞ goes from $R_\infty = \gamma$ for high λ_c to $R_\infty = 0$ for low λ_c. Thus, if the force of infection in the uncontrolled region is high, few benefits can be gained from the disease control strategy when mobility is low. On the other hand, if the force of infection in the uncontrolled region is low, a larger benefit is achieved when the mobility is high. Therefore, the disease control strategy is particularly effective when the individual mobility is high and the force of infection is highly heterogeneous. In this case, the area to be targeted is clearly defined. On the contrary, reducing the mobility (quarantine) has a general positive effect on epidemic control, but this appears not always to be suitable, since the global epidemic threshold is given by a small fraction ($p_j \simeq 10^{-2}$ in Fig. 3) of individuals performing long-distance jumps.

Finally, we briefly comment on models with temporary immunity, that is, SIRS models, which are appropriate to model endemic diseases such as influenza [37]. In this case, the immunity which is acquired after the infection is not permanent, and individuals move back to the susceptible class when the immunity vanishes. Temporary immunity is studied by introducing a further transition from the R to the S state

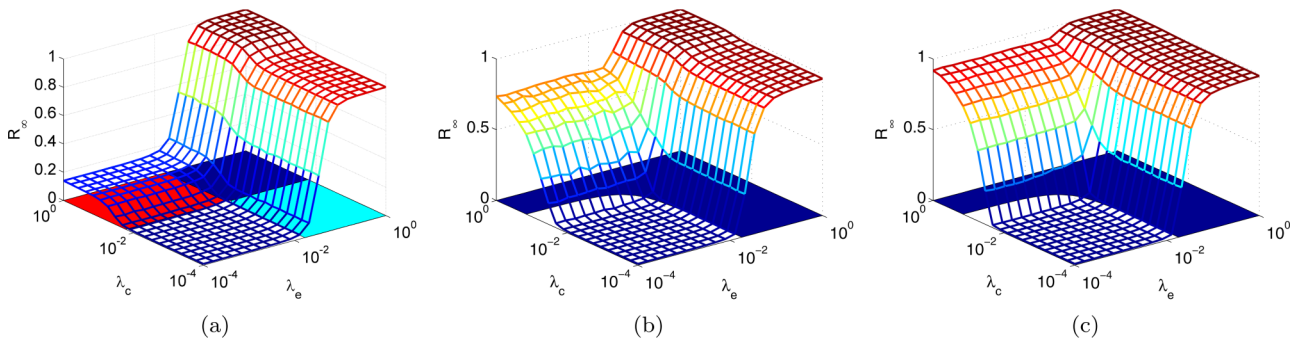

FIG. 5. (Color online) Steady-state fraction of recovered individuals R_∞ as a function of the parameters λ_c and λ_e for agents with velocities drawn from a truncated power-law distribution. We have considered a system with $N = 10\,000$, $\rho = 3$, $D = 1$, $v = 0.1$, $\mu = 0.15$, $\gamma = 1/9$, and different values of p_j: (a) $c = 0.01$, (b) $c = 0.1$, and (c) $c = 1$. The floor represents theoretical expectations. In (a) the left (red) floor region corresponds to the occurrence of condition (5) in Γ_c; the right (cyan) region, in $\Gamma\backslash\Gamma_c$; and the top (dark-blue) region, in both Γ_c and $\Gamma\backslash\Gamma_c$. In (b) and (c) the dark floor area corresponds to condition (4) being satisfied (epidemic outbreak); the white area, to condition (4) not being satisfied (no epidemic outbreak). Simulations start with 1% of the agents set to the infective state. Results are averages over 50 runs.

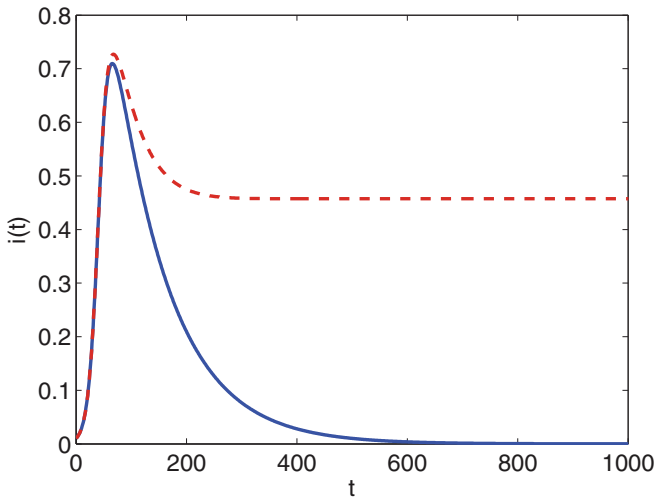

FIG. 6. (Color online) Comparison of the trend of the fraction $i(t)$ of infected individuals in the SIR [solid (blue) line] and SIRS [dashed (red) line] models with $\lambda_c = 0.1$, $\lambda_e = 10^{-2}$, $\rho = 2$, $\mu = 0.01$, $\gamma = 1/9$, and $\alpha = 0.01$. The system is started with 1% of the agents set in the infective state.

governed by a rate α, also known as the loss-of-immunity rate [37]. The average immunity period is defined as $1/\alpha$ (immunity becomes permanent for $\alpha = 0$). Under the HM hypothesis, the mean-field approximation for the SIRS model reads

$$\begin{aligned} i(t+1) &= i(t) + \gamma s(t)[1-(1-\lambda_c i(t))^a] \\ &\quad + (1-\gamma)s(t)[1-(1-\lambda_e i(t))^a] - \mu i(t), \\ r(t+1) &= r(t) + \mu i(t) - \alpha r(t), \\ s(t+1) &= 1 - i(t+1) - r(t+1). \end{aligned} \tag{6}$$

Model (6) is similar to Eq. (2), except for the presence of the term $-\alpha r(t)$, accounting for the fraction of recovered individuals which move back to the susceptible state. Using the same line of argument adopted for the SIR model, it can be found that the threshold is given, also in this case, by Eq. (4). This finding is supported by other studies on SIRS models that obtained the same result [37]. However, for the SIRS model an endemic state with a nonzero steady-state value of infected individuals is asymptotically reached. An example is illustrated in Fig. 6, which compares the trends of the fraction $i(t)$ of infected individuals in the SIR and the SIRS models. During the first part of the simulation the fractions of infected individuals in the two models grow following similar trends, whereas the steady-state values are different: $i(t)$ asymptotically vanishes in the SIR model, whereas it approaches a nonzero level in the SIRS model. The effect of the motion parameters such as p_j and v is analogous to what is observed in the SIR model.

IV. CONCLUSIONS

We have studied epidemic spreading in a population of agents moving in a heterogeneous space. In particular, we have considered a network of agents that move on a plane divided into two regions, each characterized by a different force of infection. Epidemic spreading in this system undergoes two regimes: one in which outbreaks are restricted to only one of the two regions and one in which the epidemic spreads through the whole population. We have derived a mean-field model from which the conditions that govern the onset of the epidemic in both regimes were found. The role of key parameters has also been elucidated. The force of infection, the probability of recovery, the ratio of the areas of the two regions, and the agent density determine the condition for the onset of the epidemic, computed under the hypothesis of HM. On the other hand, mobility parameters such as the agent velocity and the jump probability regulate agent mixing, and it has been found that an increased degree of mobility drives the system towards a regime in which macroscopic outbreaks appear. The threshold derived under the HM hypothesis is a lower bound for the epidemic threshold under large time scales of motion (that is, when mixing is no more homogeneous), since in this case the number of contacts decreases and the epidemic threshold increases.

Our model is of interest for the study of epidemic spreading in areas with a homogeneous agent density and for applications such as epidemic routing, an approach for sparse and/or highly mobile networks, where packets are routed from agent to agent with a mechanism analogous to infection spreading. Supposing that communications from the external world to agents are restricted to a portion of the available space, which corresponds to Γ_c in our model, then our results indicate that even if the strength of infection in Γ_c is increased to its maximum ($\lambda_c = 1$, that is, a perfect communication without packet losses), this may not suffice to achieve a macroscopic outbreak and so, in terms of the envisaged application, to implement an effective routing strategy.

[1] V. Colizza and A. Vespignani, Phys. Rev. Lett. **99**, 148701 (2007).
[2] A. Apolloni, C. Poletto, J. J. Ramasco, P. Jensen, and V. Colizza, Theor. Biol. Med. Model. **11**, 3 (2014).
[3] S. Meloni, N. Perra, A. Arenas, A. Gómez, Y. Moreno, and A. Vespignani, Sci. Rep. **1**, 62 (2011).
[4] S. Eubank, H. Guclu, V. S. Anil Kumar, M. V. Marathe, A. Srinivasan, Z. Toroczkai, and N. Wang, Nature **429**, 180 (2004).
[5] M. L. Ciofi degli Atti, S. Merler, C. Rizzo, M. Ajelli, M. Massari, P. Manfredi, C. Furlanello, G. Scalia Tomba, and M. Iannelli, PLoS ONE **3**, e1790 (2008).
[6] M. Ajelli and S. Merler, J. Theor. Biol. **259**, 478 (2009).
[7] M. Ajelli, B. Goncalves, D. Balcan, V. Colizza, H. Hu, J. J. Ramasco, S. Merler, and A. Vespignani, BMC Infect. Dis. **10**, 190 (2010).
[8] M. Frasca, A. Buscarino, A. Rizzo, L. Fortuna, and S. Boccaletti, Phys. Rev. E **74**, 036110 (2006).

[9] A. Buscarino, L. Fortuna, M. Frasca, and V. Latora, Europhys. Lett. **82**, 38002 (2008).
[10] D. Balcan and A. Vespignani, J. Theor. Biol. **293**, 87 (2012).
[11] N. Perra, B. Goncalves, R. Pastor-Satorras, and A. Vespignani, Sci. Rep. **2**, 469 (2012).
[12] N. M. Ferguson, D. A. T. Cummings, S. Cauchemez, C. Fraser, S. Riley, A. Meeyai, S. Iamsirithaworn, and D. S. Burke, Nature **437**, 209 (2005).
[13] V. Colizza, A. Barrat, M. Barthelemy, A.-J. Valleron, and A. Vespignani, PLoS Med. **4**, e13 (2007).
[14] J. M. Epstein, D. M. Goedecke, F. Yu, R. J. Morris, D. K. Wagener, and G. V. Bobashev, PLoS ONE **2**, e401 (2007).
[15] T. Graske, J. Legrand, C. A. Donnelly, H. Ward, S. Cauchemez, C. Fraser, N. M. Ferguson, and A. C. Ghani, BMJ **339**, b2840 (2009).
[16] D. Balcan, H. Hu, B. Goncalves, P. Bajardi, C. Poletto, J. J. Ramasco, D. Paolotti, N. Perra, M. Tizzoni, W. Van den Broeck, V. Colizza, and A. Vespignani, BMC Med. **7**, 45 (2009).
[17] M. Lipsitch, M. Lajous, J. J. O'Hagan, T. Cohen, and J. C. Miller, PLoS ONE **4**, e6895 (2009).
[18] R. Pastor-Satorras and A. Vespignani, Phys. Rev. Lett. **86**, 3200 (2001).
[19] A. L. Lloyd and R. M. May, Science **292**, 1316 (2001).
[20] M. E. J. Newman, Phys. Rev. E **66**, 016128 (2002).
[21] Y. Moreno, R. Pastor-Satorras, and A. Vespignani, Eur. Phys. J. B **26**, 521 (2002).
[22] M. Barthélemy, A. Barrat, R. Pastor-Satorras, and A. Vespignani, Phys. Rev. Lett. **92**, 178701 (2004).
[23] J. Gomez-Gardenes, V. Latora, Y. Moreno, and E. Profumo, Proc. Natl. Acad. Sci. U.S.A. **105**, 1399 (2008).
[24] S. Meloni, A. Arenas, and Y. Moreno, Proc. Natl. Acad. Sci. U.S.A. **106**, 16897 (2009).
[25] G. Viswanathan, S. V. Buldyrev, S. Havlin, M. Da Luz, E. Raposo, and H. E. Stanley, Nature **401**, 911 (1999).
[26] M. Lomholt, K. Tal, R. Metzler, and K. Joseph, Proc. Natl. Acad. Sci. U.S.A. **105**, 11055 (2008).
[27] A. Baronchelli and F. Radicchi, Chaos Solitons Fractals **56**, 101 (2013).
[28] D. A. Raichlen, B. M. Wood, A. D. Gordon, A. Z. P. Mabulla, F. W. Marlowe, and H. Pontzer, Proc. Natl. Acad. Sci. U.S.A. **111**, 728 (2014).
[29] K. J. Sharkey, J. Math. Biol. **57**, 311 (2008).
[30] I. Belykh, V. Belykh, and M. Hasler, Physica D **195**, 188 (2004).
[31] M. Porfiri, D. J. Stilwell, E. M. Bollt, and J. D. Skufca, Physica D **224**, 102 (2006).
[32] M. Porfiri, Phys. Rev. E **85**, 056114 (2012).
[33] M. Hasler, V. Belykh, and I. Belykh, SIAM J. Appl. Dynam. Syst. **12**, 1031 (2013).
[34] M. Frasca, A. Buscarino, A. Rizzo, and L. Fortuna, Phys. Rev. Lett. **108**, 204102 (2012).
[35] M. Barthélemy, Phys. Rep. **499**, 1 (2011).
[36] R. Pastor-Satorras, C. Castellano, P. Van Mieghem, and A. Vespignani, arXiv:1408.2701v1.
[37] H. W. Hethcote, Math. Biosci. **28**, 335 (1976).